Turkish Journal of Electrical Engineering & Computer Sciences

http://journals.tubitak.gov.tr/elektrik/

Research Article

Turk J Elec Eng & Comp Sci
(2020) 28: 34 – 44

doi:10.3906/elk-1901-134

# Simulation and analysis of wind turbine radar echo based on 3-D scattering point model

**Jiangong ZHANG**[1,2], **Bin HAO**[2,*], **Bo ANG**[2], **Li HUANG**[2], **Jiawei YANG**[2]

[1]State Key Laboratory of Power Grid Environmental Protection,
Wuhan Branch of China Electric Power Research Institute, Wuhan, PR China

[2]College of Electrical Engineering and Renewable Energy, China Three Gorges University, Yichang, Hubei, PR China

**Received:** 19.01.2019 • **Accepted/Published Online:** 21.08.2019 • **Final Version:** 27.01.2020

**Abstract:** Wind turbine (WT) arrays in wind farms can cause serious interference on nearby radar stations. This interference could be filtered out if wind turbine radar echo (WTRE) can be obtained accurately. Considering the singleness of in-field experiments, numerical simulation became the majority among such works, but few of them reached necessary accuracy. Therefore, we propose a solution method of WTRE based on three-dimensional (3-D) scattering point model. Firstly, we use the nonuniform rational B-spline to build the 3-D model of WT. Secondly, based on the method of moments (MoM), the Rao-Wilton-Gisson (RWG) basis function is adopted to discretize the integral area of WTRE into triangular elements, which ensures the continuity of induced current on the surface of WT. Taking the centers of triangular elements as scattering point source, we obtain the 3-D point scattering model of WT, which is then used to derive the echo equation of WT and eventually time-frequency domain waveform of WTRE. The result presents high accuracy comparing with the traditional method and scaled model experiments in an anechoic chamber. Further analysis indicates that the proposed method can be used to estimate important parameters of an operating WT accurately.

**Key words:** Experimental measurement, scattering point model, wind turbine radar echo

## 1. Introduction

Wind power received great attention worldwide as a promising clean energy resource [1–3]. However, for wind turbines (WTs), increased capacity normally comes with increased size, and this will probably enlarge the interference of wind farms on nearby radars, which has been reported and studied [2]. The surface of WT generates induced current under the irradiation of high-frequency electromagnetic waves, then passively emits secondary radiated electromagnetic waves back to radar devices and may cause false radar alarms [4].

Some studies were proposed to deal with this radar interference from WTs. They could be divided into two categories roughly based on the difference in targets. One is to deal with the WTs by reducing their radar cross section (RCS) [5], for example to paint materials absorbing electromagnetic waves on WT blades [6]. The other one is to deal with radar by filtering WT clutters from radar echoes, which is based on acquiring the unique Doppler features of wind turbine radar echoes (WTRE) [7–9]. While it is difficult to apply the methods of reducing RCS effectively in real wind farms [7], current research has mainly focused on obtaining WTRE accurately [8–13].

*Correspondence: 916920262@qq.com

The experimental measurements of WTRE were facing problems including high cost, complicated process, and inconvenient modification of model parameters [9, 10]. As a result, people tended to develop numerical methods to simulate and obtain the Doppler features of WTRE [10–12], and then verify the results with experiments.

Due to the huge size of WT and the high frequency of radar, the mathematical models involved in WTRE simulation are actually electromagnetic scattering problems of electrically large-sized items; thus, they are hard to solve using the method of moments (MoM) [13]. Therefore, the method of scattering point model was proposed in [10–12], which uses a set of linear disperse points to represent WT and simulate WTRE. This method is efficient in computation, but its accuracy is relatively low because the line model of WT is too rough to reflect the actual shape of WT. Though a developed model using rectangular plane to represent WT blade was proposed later in [14], but still its accuracy was not enough.

Therefore, we decided to build a 3-D surface model of WT with complex turbulence surfaces, and then use RWG basis function to discretize the whole integral area of WTRE based on MoM. Comparisons with experimental results obtained in anechoic chamber and traditional methods show that the proposed 3-D model of WTRE is improved in both accuracy and calculation speed.

## 2. Acquisition of equivalent scattering point of WT

### 2.1. Traditional solution method of WTRE

Based on the theory of electromagnetic field, WT could be taken as a collection of charged particles in EM calculations. The high-frequency incident electromagnetic waves emitted by radar will interact with these charged particles, and generate new equivalent charges, currents, magnetic charges, magnetic currents, and new field sources that distributed on the surface of WT. The surface electric field integral equation is proposed in [15].

Normally it is difficult to obtain accurate analytical results of the integral equation due to the rather complicated structure of WT. Therefore, numerical methods such as MoM and the RWG basis function are used to disperse the integral equation. However, because the radar frequency is usually over GHz, the calculation using MoM is quite difficult to finish since it requires too much computation resource.

As a result, the scattering point model for simulating WTRE based on the basic equations of radar echo is proposed [10–12]. As shown in Figure 1, the static stance of WT at any fixed moment is taken to perform geometric modeling of WT in a coordinate system, where the center point of WT blade is set to be the origin of the coordinate system and the $x$-axis is perpendicular to the blade rotation plane. Then the expression of radar echo from any point target was obtained in [12]:

$$S_{\mathrm{np}}(t) = \exp(\mathrm{j}(2\pi f_{\mathrm{c}} t - 4\pi \frac{R}{\lambda})), \tag{1}$$

where $f_c$ and $\lambda$ are the frequency of the radar transmission signal and the radar operating wavelength, respectively, $R$ is the distance from the scattering point of WT to the radar and it appears to be the decisive parameter affecting radar echo.

In the earliest scattering point model, a WT is equivalent to a simple cylinder with three blades and a tower, and the cylinders are evenly divided into thin wafers. Then it uses points of the wafer centers to replace

the thin wafers. As a result, WTRE of the whole WT is equivalent to the sum echo from the large number of scattering points linearly distributed [10–12]. Finally, the echo of WT can be obtained as follows:

$$S_{\mathrm{i}}(t)=\int_0^L \exp(\mathrm{j}\frac{4\pi l_{\mathrm{i}}\cos\varphi}{\lambda})\mathrm{d}l_{\mathrm{i}}+\int_0^H \exp(-\mathrm{j}\frac{4\pi h_{\mathrm{i}}\cos\beta}{\lambda})\mathrm{d}h_{\mathrm{i}}, \tag{2}$$

where $S_i(t)$ is the echo baseband signal of any scattering point; $t$ is time; $\varphi$ is the angle between the blade and the Line of Sight (LOS); $\beta$ is the pitch angle of radar; $l_i$ and $h_i$ are the distances from the scattering points $B_i$ and $T_i$ to the origin of the coordinates, respectively; $\lambda$ is the wavelength of radar; $L$ and $H$ are the WT blade length and the tower height, respectively.

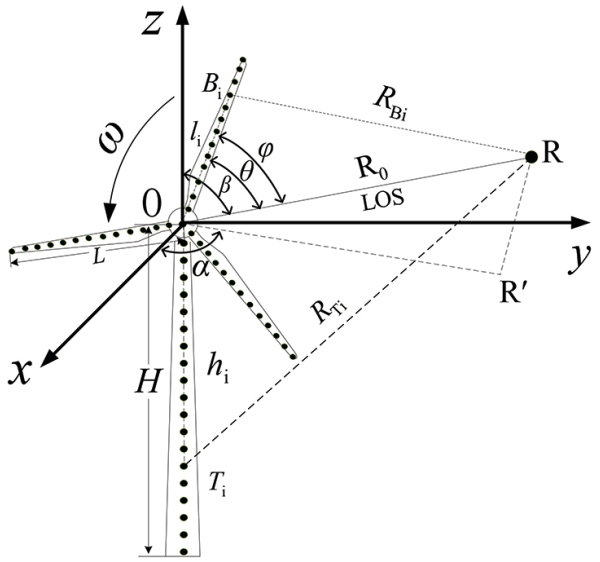


**Figure 1**. WT and radar position diagram.

Integral calculation of Equation 2, and addition of carrier terms and constant phase terms yields an overall WTRE expression with $K$ blades:

$$\begin{aligned}S_{\mathrm{WT}}(t)=&S_{\mathrm{B}}(t)+S_{\mathrm{T}}(t)\\&=\exp(\mathrm{j}2\pi f_{\mathrm{c}}t)\cdot\exp(-\mathrm{j}\frac{4\pi R_0}{\lambda})\cdot\\&\left\{\sum_{\mathrm{k}=1}^{K}L\exp\left[\mathrm{j}\frac{2\pi L}{\lambda}\cos\varphi_{\mathrm{k}}(t)\right]\mathrm{sinc}\left[\frac{2L}{\lambda}\cos\varphi_{\mathrm{k}}(t)\right]+H\exp\left(-\mathrm{j}\frac{2\pi H}{\lambda}\cos\beta\right)\mathrm{sinc}\left(-\frac{2\mathrm{H}}{\lambda}\cos\beta\right)\right\},\end{aligned} \tag{3}$$

where $S_{WT}(t)$ is the overall WTRE; $S_B(t)$ is the WTRE about blade; $S_T(t)$ is the WTRE about tower; $f_c$ and $\lambda$ are the center frequency and wavelength of the radar transmit signal, respectively; $R_0$ is the distance from the radar to the center of the blade; $K$ is the number of blades of the WT.

This method has high computational efficiency, but its result is obviously poor in accuracy due to its rough equivalent to actual WTs. Then there is the model with a rectangular plane to represent the WT blade [14], but the plane surface in this model cannot be used to simulate WTRE accurately either.

Eventually building a 3-D model of WT to reflect its actual external structure becomes a reasonable solution for us. We will also need a method to disperse the model into equivalent scattering elements to calculate WTRE. Especially, the continuity of induced current should be ensured for the simulation accuracy.

### 2.2. Establishment of the 3-D WT model

According to the structural characteristics of blade, the 3-D model of blade is established by using the nonuniform rational B-spline (NURBS) [16]. Before modeling the NURBS surfaces, it is necessary to know the coordinate parameters of the blade elements.

When the blade airfoil is determined, the standard airfoil section coordinate of $(x_0, y_0)$ and the blade's aerodynamic center coordinate of $(X, Y)$ are fixed values, and the airfoil has the aerodynamic center as the origin coordinate $(x_1, y_1) = (x_0, y_0) - (X, Y)$. To solve the 3-D coordinates of the blade, it is necessary to consider the influence of the blade torsion angle. The angle between any point on the blade element and the x-axis is $\arctan(y_1/x_1) + \theta$. Therefore, the point coordinates of the blade element disperse space are:

$$\begin{cases} x = C\sqrt{x_1^2 + y_1^2}\cos\{\arctan(y_1/x_1) + \theta\} \\ y = C\sqrt{x_1^2 + y_1^2}\sin\{\arctan(y_1/x_1) + \theta\} \\ z = L \end{cases} \tag{4}$$

Here $C$ and $\theta$ are respectively expressed as the chord length and torsion angle of the blade element, $L$ is the length of the blade.

By establishing the space coordinates $(x, y, z)$ of the blade with a NURBS surface, the corresponding 3-D model of the blade can be obtained. Then with the other static components, the 3-D model of WT is set up as shown in Figure 2.

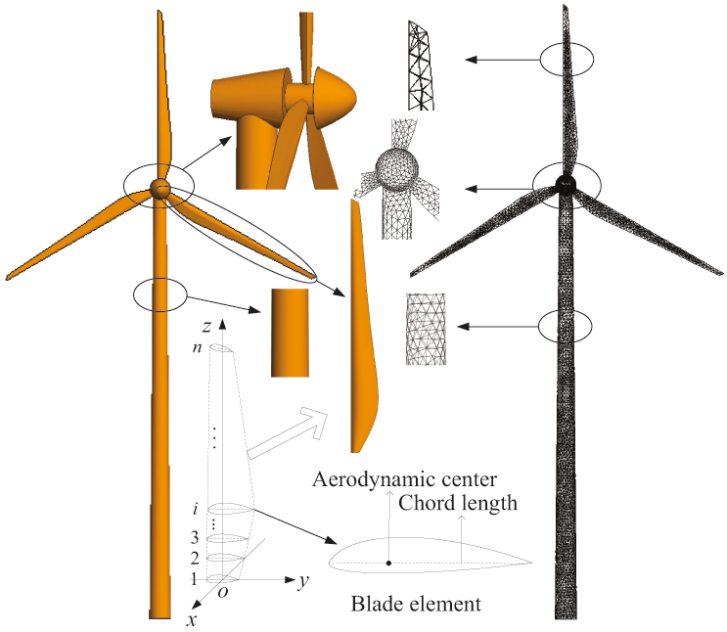


**Figure 2**. 3-D model and triangular facet segmentation results of WT.

### 2.3. Acquisition of WT scattering points

To acquire the scattering points of 3-D WT accurately while ensuring the continuity of induced current, we use the RWG basis function to disperse the electric field integral equation, which means using triangle surface elements to divide the whole surface model of WT into a collection of triangular elements, as shown in Figure 2. Each triangular element is a field source of electromagnetic scattering, and the whole WTRE could be represented by the echo sum from all the triangular elements. Taking the center of the triangular element as the scattering point source, we can acquire the coordinates of equivalent scattering points. In this way, the point scattering model representing the 3-D WT is established.

## 3. Solution of WTRE

### 3.1. Derivation of WTRE formula

In order to obtain radar echoes of all the scattering points from WT, it is necessary to solve the decisive parameter $R$ in Equation 1, which belongs to the problem of the distance between two points. Here $R$ is determined as:

$$R_{\mathrm{P_i}}(t) = \sqrt{(x_{\mathrm{B}} - x_{p_i})^2 + (y_{\mathrm{B}} - y_{p_i})^2 + (z_{\mathrm{B}} - z_{p_i})^2}, \tag{5}$$

where $x_B$, $y_B$, and $z_B$ are the radar coordinate scales; $x_{P_i}$, $y_{P_i}$, and $z_{P_i}$ represent the coordinate scales of scattering points.

For a rotating WT blade, the coordinate positions of the scattering points constituting the blade change continuously. Assuming that a certain scattering point $(x_0, y_0, z_0)$ on the WT rotates with the blade for $\Delta t$, then it is not difficult to obtain its new coordinates $(x_t, y_t, z_t)$ as shown in Equation 6.

$$\begin{cases} x_t = x_0 \\ y_t = \sqrt{(x_0^2 + y_0^2 + z_0^2)}\cos(2\pi\omega\Delta t + \psi) \\ z_t = \sqrt{(x_0^2 + y_0^2 + z_0^2)}\sin(2\pi\omega\Delta t + \psi) \end{cases} \tag{6}$$

where $\omega$ represents the blade rotation angular velocity, $\psi$ represents the angle made of the scattering point $(x_0, y_0, z_0)$, the origin line and the y-axis. When $z_0 > 0$, $\psi = \arccos(y_0/l_0)$; when $z_0 \leq 0$, $\psi = \arccos(y_0/l_0) + \pi$. Assuming that the WT blade consists of $M$ scattering points, the overall echo of the blade can be expressed as:

$$S_{\mathrm{blade}}(t) = \sum_{i=1}^{M} \exp\left(\mathrm{j}\left(2\pi f_c t - \frac{4\pi R_{P_i(t)}}{\lambda}\right)\right). \tag{7}$$

For the stationary tower, its scattering points do not move with time. Therefore, the model of tower echo is similar to that of a blade at a certain moment. Assuming that the tower is composed of $N$ scattering points, its echo is:

$$S_{\mathrm{mast}}(t) = \sum_{i=1}^{N} \exp\left(\mathrm{j}\left(2\pi f_c t - \frac{4\pi R_{Q_i}}{\lambda}\right)\right). \tag{8}$$

Finally, the WTRE could be obtained as the sum of radar echoes of the blades and the tower.

### 3.2. WTRE solving process

Since WT blades are rotating all the time, we use the quasistatic method to solve WTRE in one rotation period, as shown in Figure 3. Meanwhile, the echo of tower only needs to be calculated once. The whole calculation of WTRE can be regarded as knowing all the scattering points coordinates of WT and the position of radar to solve Equations 6 and 7.

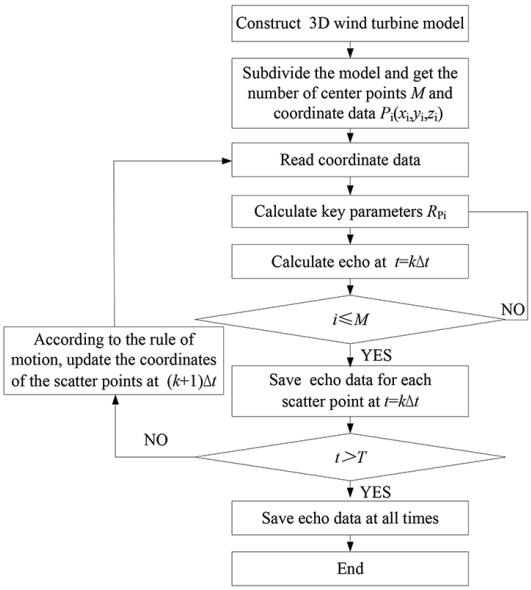


**Figure 3**. Calculation flow chart of WTRE.

Considering that the short-time Fourier transform (STFT) does not generate cross-interference when processing multicomponent signals, it is adopted in this paper to obtain the WT echo time-frequency domain waveform (TFDW), which is defined as:

$$STFT_s(t,\omega) = \int_{-\infty}^{+\infty} s(\tau)h(\tau - t)\cdot \mathrm{e}^{-i\omega\tau}\mathrm{d}\tau, \tag{9}$$

where $h(t)$ is the window function used in the STFT, which is the Gaussian window function here.

## 4. Simulation and experiment

### 4.1. WTRE simulation

Jinfeng 77/1500 is a common model of WT widely used in wind farms in China. Thus, it is chosen as the target WT in this paper. For Jinfeng 77/1500, its WT blade length is 74.6 m, the airfoil model is NACA4412, and the tower height is 85 m. Using the method described in Section 2, the model is established and scattered according to the size of $\lambda/10$, and the total number of scattering points is 54,571.

The simulation parameters are shown as follows: the length of WT blade $L = 36.5$ m, the height of tower $H = 84$ m, the rotation speed of WT blade $\omega = 26\mathrm{r/min}$, the radar transmission frequency $f_c = 10$ GHz, the pulse repetition rate $PRF = 1000\,\mathrm{Hz}$ and the observation time $T = 2.3$ s which is normally a rotation period.

Using the traditional method mentioned in Section 2, the time domain waveform (TDW) and TFDW of WTRE were obtained as shown in Figure 4.

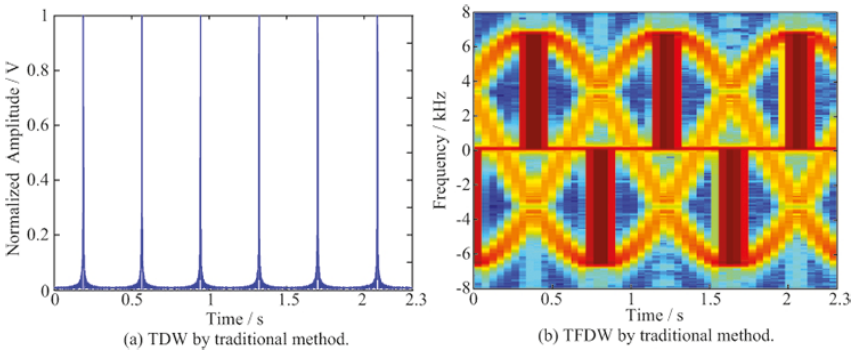


**Figure 4**. Simulation results of the traditional method.

As can be seen from Figure 4a, a total of six peaks appear in the TDW diagram of WTRE in one rotation period. Combining the initial stance of blades, the TDW indicates that the peaks appear when one blade is perpendicular to the incident direction of radar electromagnetic wave; thus, each blade appears twice in one rotation period.

Comparing Figures 4a and 4b, it is easy to see that the moment of flash in the TFDW diagram and the moment of peak in the TDW diagram are identical to each other. The amplitude of the sinusoidal envelope curve caused by rotating blades corresponds to the positive and negative Doppler frequency shifts in the TFDW diagram, which is different from tower and nacelle. The contribution of tower and nacelle in the TFDW is the zero frequency band, which is very similar to the general grand clutters.

At the same time, the time domain waveform (TDW) and TFDW of WTRE were obtained by using this paper's method mentioned in Section 3 as shown in Figure 5.

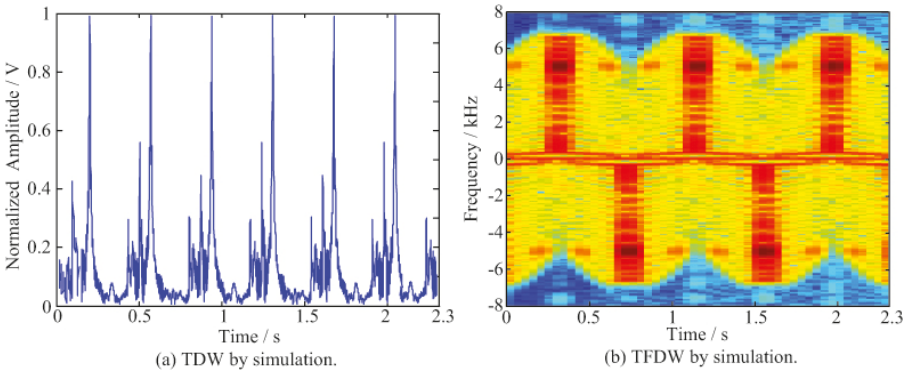


**Figure 5**. Simulation results by paper's method.

Comparing Figures 4 and 5, the curve of the time domain peak has a very large difference under the same parameter conditions. In Figure 4, there is a single peak in the time domain peak, and in Figure 5, in addition to a sharp peak, there are many small peaks. These small peaks are due to the 3-D model considering the shape of WT. When the blade rotates close to LOS of the radar, a small amount of partial scatter points appears perpendicular to the LOS early or late, and these small peaks are formed by the superposition of their echoes. The subpeaks occurred near the peak, and the curve characteristics of TDW near the peak are quite typical and that could be used to characterize the profile of WT blade. They have been applied in the fault detection of WT in some recent research [14].

Comparing Figures 4 and 5, it can be seen that the Doppler feature in the time-frequency domain waveform diagram still exists. In contrast, there is only one sinusoid in Figure 4, which is formed by the tip of the blade; the sinusoid in Figure 5 has many strips. Since each part of the blade provides scattering, there is a difference in the Doppler frequency generated by the rotation of the different parts. Therefore, the sinusoidal envelope domain in Figure 5 appears.

From the clutter filtering work in [17, 18], ignoring the Doppler features appearing in the above echoes will seriously influence the filtering effect of wind turbine clutter and even make the whole clutter filtering work impossible.

### 4.2. Experimental measurement of WTRE

To verify the accuracy of the proposed simulation method, we measured the WTRE of WT in an anechoic chamber using a scaled model. The experimental platform is shown in Figure 6, and the experimental parameters are as follows: the length of WT scaled model blade $L' = 0.61$ m, the height of its tower $H' = 1.40$ m, the rotation speed of WT scaled model blade $\omega' = 26$ r/min, the radar transmission frequency in experimental measurement $f_c' = 10$ GHz, the pulse repetition rate of pulse wave $PRF' = 1000$ Hz and the observation time $T' = 2.3$ s which is normally a rotation period of WT-scaled model blade. To obtain the electromagnetic scattering data of scaled model accurately, it is necessary to measure a standard ball with known RCS firstly. This step called "calibration" is taken to not only eliminate the interference from background noise, but also to set the "distance gate" that prevents the interference caused by other targets.

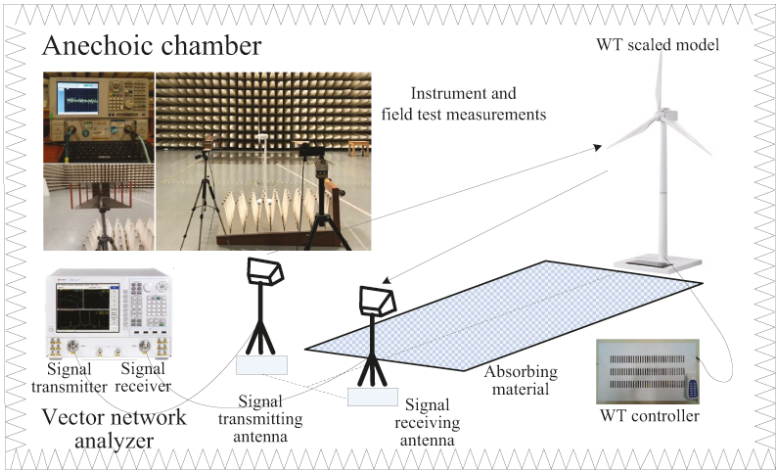


**Figure 6**. Experimental measurement platform.

The testing site in anechoic chamber is shown in Figure 6. AV3672C-S vector network analyzer was used. After setting up the experimental platform, relevant parameters were set firstly, including the electromagnetic wave emission frequency and polarization mode, sampling points, and sampling frequency. It should be noted that polarization was divided into vertical polarization and horizontal polarization and the measurement data in this paper were all vertical polarization. In addition, the number of sampling points was set artificially taking it into account that the measurement accuracy and test time both increase with it. The sampling frequency was set indirectly by setting the IF bandwidth considering that the Nyquist sampling law had to be satisfied. The WT blade rotation was remote-controlled. After the rotation speed was stable, the relevant data were measured and exported. The measurement results are shown in Figure 7.

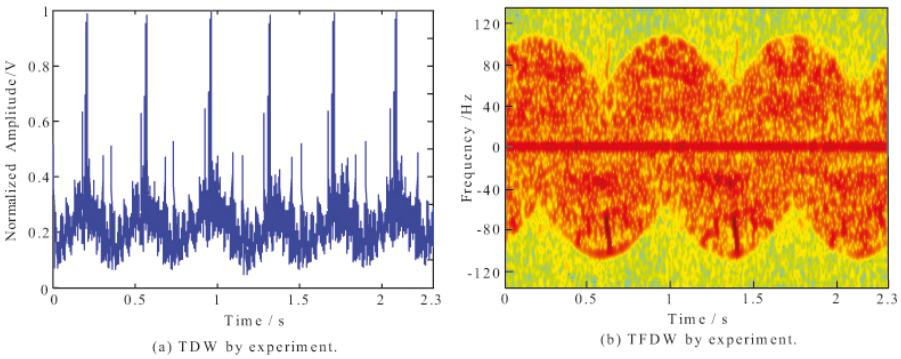


**Figure 7**. Experimental measurement results.

### 4.3. Experiment results analysis

Comparing Figure 5a with Figure 7a, it can be seen that the moment and the number of peaks generated in the TDW diagram are the same, and the two parameters are specific representations of the Doppler effect in the TDW diagram. The small difference in time between the time domain peaks in Figure 5a and Figure 7a are caused by interference from experimental instruments and environment.

Comparing Figure 5b with Figure 7b, it can be found on the time axis that the sinusoidal envelope curves reach the peaks and troughs at the same time. Comparison on the frequency axis shows that the Doppler frequency of the experimental measurement is much smaller than the Doppler frequency obtained by the numerical calculation.

We discussed the reason for the difference in Doppler frequency from the aspects of WT parameters and the definition of Doppler frequency. The Doppler frequency is proportional to the maximum linear velocity of the rotating target [11]. Meanwhile the maximum linear velocity of blade is proportional to blade length for a fixed rotational speed. That means the Doppler frequency is proportional to blade length. According to the parameters in the comparison between simulation and experiment, the Doppler frequency calculated by numerical calculation should be 36.5/0.61 times that of the experimental measurement. As shown in Figures 5b and 7b, it is easy to see that their corresponding Doppler frequencies are $f_1 = 6.62$ kHz and $f_2 = 113.21$ Hz, respectively, which are quite consistent with the proportional relationship between Doppler frequency and blade length.

## 5. Parameter estimation and analysis

Another important application of WTRE is to estimate the operating parameters of blades using Doppler characteristics of WTRE. As can be seen from Figure 5a, it takes 1.11 s for blades to rotate 120°, which indicates the rotational speed of blade to be 26.79 r/min. As can be seen from Figure 7b, the Doppler frequency of the WTRE is 6.62 kHz, and the Doppler frequency of WTRE is

$$f_d = 4\pi\omega\frac{L}{\lambda}. \tag{10}$$

The length of blade can be estimated based on Equation 10. In summary, WT parameters estimated from simulation results are shown in Table.

As can be seen from Table, the number of WT blades is estimated accurately. There are small errors in blade speed and blade length.

**Table 1**. Estimated parameters.

| | Number of blades | Spinning speed $\omega$(f/min) | Blade length $L$(m) |
|---|---|---|---|
| True | 3 | 26.09 | 36.50 |
| Estimate | 3 | 26.79 | 37.86 |

For the estimation of blade rotation speed, the time domain peak appears when the blade is perpendicular to the incident direction of radar electromagnetic wave, the echo phases of each scattering point are similar and the echo energy is superposed. Considering the blade profile, the moment of the highest energy is not exactly the moment when the centerline of the blade is perpendicular to the line of sight of radar. This caused the small error in the rotation speed.

For the estimation of blade length, the estimated value is bigger than the actual value. The $f$d read from the time frequency domain echo pattern is slightly larger than the Doppler frequency domain generated by the linear blade. This is mainly because the scattering point on the blade located farthest from the hub generates the maximum Doppler frequency shift. The longest distance is not provided by the centerline of blade, but by other lines that are slightly offset from the centerline, which results in excessively long blade length estimation.

## 6. Conclusions

1) The 3-D scattering points model of WT ensuring the continuity of the scattered current on the surface of WT can accurately obtain the time-frequency domain information of WTRE, which can be widely used in the field of WTRE simulation and analysis. Its fidelity is confirmed by experimental measurements.

2) According to the WTRE simulation results obtained by the 3-D scattering points model of WT, the important operating parameters of WT can be predicted accurately, including the blade number, blade length, and rotation speed.

3) In actual engineering, the wind turbines are usually in groups. Based on a single WTRE simulation method proposed in this paper, the next step is to carry out the echo simulation studies about the multiple WT arrays.

## Acknowledgment

This work was supported by State Key Laboratory of Power Grid Environmental Protection under Grant GYW51201901075 and by Science and Technology Program of SGCC under Grant GY71-16-011.

## References

[1] Dai XM, Zhang KF, Geng J, Liu QQ, Wang Y et al. Study on variability smoothing benefits of wind farm cluster. Turkish Journal of Electrical Engineering and Computer Sciences 2018; 26(04): 1894-1908.

[2] Abdullah MA, Muttaqi KM, Sutanto D, Agalgaonkar AP. An effective power dispatch control strategy to improve generation schedulability and supply reliability of a wind farm using a battery energy storage system. IEEE Transactions on Sustainable Energy 2015; 6(3): 1093-1102.

[3] Ashraf MM, Malik TN. Design of a three-phase multistage axial ux permanent magnet generator for wind turbine applications. Turkish Journal of Electrical Engineering and Computer Sciences 2017; 25(01): 520-538.

[4] David DLV, Matthews J, Norin L, Angulo I. Mitigation techniques to reduce the impact of wind turbines on radar services. energies 2013; 6(06): 2859-2873.

[5] Yamazaki H, Koshiji K. Radar cross-section measurement method using a spatial filtering within a near zone. IEEJ Transactions on Electrical and Electronic Engineering 2009; 4(01): 107-113.

[6] Rashid L, Brown A. Partial treatment of wind turbine blades with radar absorbing materials (RAM) for RCS reduction. In: Proceedings of the Fourth European Conference on Antennas and Propagation; Barcelona, Spain; 2010. pp. 1-5.

[7] Tang B, Zou F, Sun ZA, Huang HS, Ye L. Solution of wind turbine blade Doppler and its characteristic analysis. The Journal of Engineering 2017; 2017(13): 1347-1350.

[8] Naqvi A, Yang ST, Ling H. Investigation of Doppler features from wind turbine scattering. IEEE Antennas and Wireless Propagation Letters 2010; 9(01): 485-488.

[9] Kong F, Zhang T, Palmer RD. Wind turbine radar interference studies by polarimetric measurements of a scaled model. IEEE Transactions on Aerospace and Electronics Systems 2013; 49(03): 1589-1600.

[10] Jung JH, Lee U, Kim SH, Park SH. Micro-doppler analysis of Korean offshore wind turbine on the L-band radar. Progress in Electromagnetics Research 2013; 143(01): 87-104.

[11] He WK, Guo SS, Wang XL, Wu RB. Micro-doppler features analysis of wind farm echoes for air traffic control radar in scanning mode. Journal of Signal Processing 2015; 31(10): 1240-1246.

[12] Chen VC. The Micro-Doppler Effect in Radar. Boston, MA, USA: Artech House, 2011.

[13] Algar MJ, Somolinos A, Moreno J. Overview of some numerical techniques for the analysis of the electromagnetic scattering by wind turbines. 2016 10th European Conference on Antennas and Propagation 2016; 1: 1-5.

[14] Crespo-Ballesteros M, Antoniou M, Cherniakov M. Wind turbine blade radar signatures in the near field: modeling and experimental confirmation. IEEE Transactions on Aerospace and Electronic Systems 2017; 53(04): 1916-1931.

[15] Tang B, Wen YF, Zhao ZB, Zhang XW. Computation model of the reradiation interference protecting distance between radio station and UHV power lines. IEEE Transactions on Power Delivery 2011; 26(02): 1092-1100.

[16] Bazilevs Y, Korobenko A, Deng XW Yan JH. Novel structural modeling and mesh moving techniques for advanced fluid-structure interaction simulation of wind turbines. International Journal for Numerical Methods in Engineering 2015; 102(03): 766-783.

[17] He WK, Guo SS, Wang XL, Wu RB. Frequency fretting feature extraction of wind farm based on singular value decomposition. Journal of Electronic Measurement and Instrument 2017; 31(04): 588-595.

[18] He WK, Zhai QP, Wang XL, Wu RB. Detection and suppression of wind farm clutter in scanning mode air traffic surveillance radar. Acta Aeronautica Sinica 2016; 37(04): 1316-1326.